Novel, cost-effective configurations of combined power plants for small-scale cogeneration from biomass: Design of the immersed particle heat exchanger

Novel, cost-effective configurations of combined power plants for small-scale cogeneration from biomass: design of the Immersed Particle Heat Exchanger

Riccardo Amirante, Elia Distaso and Paolo Tamburrano

Department of Mechanics, Mathematics and Management (DMMM),
Polytechnic University of Bari, Italy

Abstract

This paper aims at proposing a general procedure for the preliminary design of the Immersed particle heat exchanger, which is a novel high temperature gas to gas heat exchanger using ceramic particles as solid intermediate medium for the purpose of transferring heat between two gases in high temperatures applications where negligible pressure drops are needed. This work gives an insight into the application of this heat exchanger to a novel, small scale, externally fired combined cycle, providing details regarding its architecture and characteristics as well as novel solutions that can reduce the capital costs of the heat exchanger while increasing its efficiency. Analytical models are developed for the design of the systems necessary to move the particles within the heat exchanger and for the evaluation of the associated energy losses. In addition, an optimization design procedure is developed in order to correctly select the main geometric parameters of the heat exchanger with application to a generic externally fired combined cycle. The procedure is finally tested on a specific case, in which specific thermodynamic values of the externally fired combined cycle were considered. The results show that the project is highly viable, as the dimensions of the heat exchanger are compact with both the pressure and energy losses being negligible.

Keywords: biomass; combined cycle; gas to gas heat exchanger

NOMENCLATURE

c_p	*Specific heat at constant pressure*	*[J/(kg K)]*
D_{top}	*Diameter of the top column*	*[m]*
D_{bot}	*Diameter of the bottom column*	*[m]*
D_r	*Rotor diameter*	*[m]*
G_a	*Air mass flow rate*	*[kg/s]*
$G_{a,lost}$	*Total loss of compressed air*	*[kg/s]*
$G_{a,lost,1}$	*Loss of compressed air (first contribution)*	*[kg/s]*
$G_{a,lost,2}$	*Loss of compressed air (second contribution)*	*[kg/s]*
$G_{a,lost,3}$	*Loss of compressed air (third contribution)*	*[kg/s]*
G_b	*Fuel mass flow rate*	*[kg/s]*
G_p	*Particle mass flow rate*	*[kg/s]*
G_s	*Steam mass flow rate*	*[kg/s]*
H_{top}	*Height of the top column*	*[m]*

H_{bot}	*Height of the bottom column*	*[m]*
i	*Enthalpy*	*[J/kg]*
h	*Blade height*	*[m]*
n_{mod}	*Number of IPHE modules*	
p	*Static pressure*	*[Pa]*
S_{tot}	*Overall heat exchange surface*	*[m^2]*
T	*Temperature*	*[K]*
V	*Volume of the particles discharged per revolution*	*[m^3]*
W	*Blade width*	*[m]*

Greek

ε_{tol}	Tolerance
ξ	*Coefficient accounting for blade thickness*
λ	*Thermal conductivity*
λ_v	*Filling coefficient*
η_{conv}	*Efficiency of the pneumatic conveyor*
η_{IPHE}	*Efficiency of the IPHE*

Subscripts

1	*Compressor inlet*
2	*Compressor outlet*
2’	*Inlet of the bottom column*
3	*Turbine inlet*
5	*Inlet of the top column*
6	*Outlet of the top column*
bot	*Bottom of the IPHE*
top	*Top of the IPHE*
p	*Particles*
press	*Pressurization system*
sim	*Simulation*

Acronyms

CHP	*Combined heat and power*
EFGT	*Externally fired gas turbines*
HRSG	*Heat recovery steam generator*

HTHE	*High temperature heat exchanger*
IPHE	*Immersed particle heat exchanger*
ORC	*Organic Rankine Cycle*
PHS	*Particle handling systems*
RPM	*Revolutions per minute*

1. Introduction

As established by the recent 2015 United Nations Climate Change Conference held in Paris, COP 21, all nations have to promote the employment of renewable technologies in order to reduce the quantity of CO_2 released into the environment. The declared target is to limit the temperature increase to 2 °C compared to pre-industrial levels [1]. To reach this goal, it is very important to develop novel and effective technologies capable of boosting the exploitation of renewable sources [2]. Among these, biomass is the most continuous source of energy [3]; biomass can be used either directly as solid fuel feeding power plants or indirectly after conversion into a secondary form of energy (e.g. syngas and biogas) by using air, oxygen and/or steam [4]. In spite of the several advances achieved in biomass gasification systems [5], the direct use of biomass needs further developments in relation to the stat of the art. Over the past years, the industrial and university research has been focused on the development and improvement in ORC power plants, which are, at the state of the art, the most widespread and profitable technology applicable to burning biomass for small scale cogeneration (production of heat and power) [6]. Different ORC configurations were studied in [7] to exploit high temperature waste heat; in contrast, the application of ORC to low grade waste heat recovery was thoroughly investigated in [8]. The effects of the thermodynamic parameters on the ORC performance were examined in detail in [9] along with the effects of different working fluids. It results that the maximum values of electrical efficiency attained by small-scale biomass-fired Organic Rankine Cycle (ORC) systems (the leader technology for CHP generation from biomass) are lower than 20%, with the efficiency decreasing with the decreasing size of the plant [10].

The main problem regarding ORC power plants is the need for organic fluids, which usually have a global warming potential greater than zero and are usually toxic and inflammable. For these reasons, rather than focusing on the improvement in the ORC technology, the authors of this paper have been concentrating all their efforts on a different strategy, which aims at proposing a concrete alternative to ORC plants. The proposed alternative is a small-scale combined cycle employing a topping externally fired turbogas cycle followed by a bottoming steam cycle, which is capable of producing useful heat and power from solid biomass. This power plant, which was proposed in [11], has the advantage of using a natural fluid (water) instead of an organic molecule. Furthermore, the main idea is to feed this power plant with carbon neutral biomass and to position the plant on site (where the biomass is produced), thus avoiding the amount of CO_2

released into the environment because of fuel transportation (an example of carbon neutral biomass is represented by pruning residues, which are usually unemployed in spite of their large availability, especially in the Mediterranean regions [12]). These characteristics make the proposed power plant fully sustainable; in addition, the feasibility in terms of efficiency was addressed in the previous paper [11], which demonstrated that the presented combined cycle has the potential to achieve a high level of electrical efficiency (up to 25%), while being cost-effective. That analysis was performed for a very low size of the plant, namely for a produced electrical power of 100 kW_e. For such an electrical power produced from biomass, the electrical efficiency of stand-alone ORC cycles is usually well below 20% [11].

The realization of the proposed combined cycle is made possible by the external combustion configuration, in which the core is a gas to gas heat exchanger capable of coupling the turbogas with the external combustor (to be fed with carbon neutral biomass). With regard to externally fired and/or closed cycle gas turbine configurations, the studies present in the scientific literature mainly deal with the optimization of the thermodynamic parameters of the proposed solutions [13]. As an example, in [14] the optimal thermodynamic parameters were found for a plant with a power generation capacity of 1 MW and incorporating a biomass gasifier using paper as fuel. As a further example, in [15] the coupling between an 103 externally fired gas turbine and a solar collector was investigated in detail.

However, the realization of an externally fired gas turbine (and hence externally fired combined cycle) is only allowed by the presence of the gas to gas heat exchanger, and the scientific literature has not highlighted effective gas to gas heat exchangers that are also capable of withstanding very high temperatures [16]. This is due to the fact that the design of the gas to gas heat exchanger is not a trivial task, since it must ensure low pressure drops while being capable of withstanding the high temperatures developed by a turbogas cycle. Furthermore, it must be compact and able to guarantee a continuous operation mode. Unfortunately, all these characteristics are very difficult for a gas to gas heat exchanger to obtain at the same time. Technical solutions provided to date mainly refer to low temperature applications, namely, to the design of recuperators for small- and microturbines, where the employed low pressure ratios make the heat recovery mandatory. A variety of gas-to-gas recuperators were discussed in [17], in which plate, plate fin, printed circuit, and spiral and tubular heat exchangers were compared, confirming that the only way to reach very high temperatures is to use an intermediate thermal medium, made of ceramic material, first to recover and then to release heat from a high temperature flow to another one. In another study, a wide range of heat exchanger concepts and demonstrators were compared [18], confirming the highest potential of ceramic recuperators over the other ones. The main problem is that currently available ceramic heat exchangers have either a non-continuous operation mode or produce too high pressure drops. Two innovative concepts for microturbine applications were proposed recently: a ceramic honeycomb regenerator disk [18] and the novel "Swiss-Roll" [19]. In the former, the ceramic honeycomb is the thermal vector able to absorb heat from the hot flow and to release it to the cold flow, passing alternatively into a rotating structure. The latter is made up of "two flat plates that are wrapped around each other, creating two concentric channels of rectangular cross-section" [19]: the theoretical efficiency of this heat exchanger is 85%, but with a pressure drop of 10%. A similar architecture, developed by Zimmermann et al. [20], is composed of two ceramic tanks that are periodically switched to allow the heat exchange between hot and cold gases. This configuration has the drawback of being discontinuous.

Because of the typical drawbacks caused by the employment of ceramic materials (high pressure drops and discontinuous operation), some studies are investigating on valid alternatives to ceramic materials, such as new alloys capable of withstanding very high temperatures and pressures [21].

In this scenario, because of the lack of available gas to gas heat exchangers capable of both withstanding high temperatures and producing negligible pressure drops as well as working continuously, two configurations for the gas to gas heat exchanger were proposed by the authors in the previous paper, with the first one being based on a conventional tube and shell configuration made of a highly-resistant metallic alloy, such as a nickel alloy. This solution has a limitation regarding the maximum temperature reachable at the inlet of the gas turbine, which results in a limitation in the maximum cycle efficiency. For this reason, another solution was also proposed for the gas to gas heat exchanger, named the immersed particle heat exchanged (IPHE). The IPHE employs ceramic particles as an intermediate solid medium with high thermal capacity: the particles fall in a column where the combustion gases flow from the bottom to the top; the warmed up particles are then collected at the bottom of the column and inserted into the top of a second column where they transfer the accumulated heat to the counterflowing cold gas, namely the compressed air coming from the compressor. By virtue of its unique characteristics (it does not make use of metallic surfaces for the heat exchange and is composed of large vertical ducts which make the pressure drops negligible), the IPHE has the potential to overcome the unresolved problems regarding gas to gas heat exchangers, namely the achievement of high temperatures and low pressure drops at the same time, while guaranteeing a continuous operation mode.

The previous paper [11] was based on the thermodynamic analysis of the small scale combined cycle; however, the design and application of the innovative heat exchanger to the combined cycle was not performed. This paper is the second part of the previous paper [11] in that gives an insight into the IPHE, providing more details regarding its architecture and characteristics, in addition to proposing a general approach for the design of its main components in the case of application to small scale externally fired combined cycles. The main objective is to find out the main dimensions (height and diameters of the heat exchanger) necessary for the heat exchange and evaluate the feasibility in terms of bulkiness and energy losses when the IPHE is applied to a specific case of study.

2. Materials and methods

This section shows the application of the IPHE to the combined cycle presented in [11], providing all the necessary details about the architecture of the IPHE. Fundamental systems serving the purpose of moving the particles inside the heat exchanger are conceived, and analytical models are developed to design these systems and study the associated energy losses. The architecture and analytical model of the heat exchange columns, which are the core of the heat exchanger, are also presented and discussed. An optimization process design is finally developed that is based on the coupling among the analytical models, a genetic algorithm and a CFD analysis of the heat exchange between the particles and the gas within both columns.

2.1 Application of the immersed particle heat exchanged to small scale combined cycles externally fired with biomass

Figure 1 shows the proposal of application to the combined cycle. The latter must be externally fired, with the input thermal power being given by the combustion of carbon neutral biomass, such as pruning residues [12]; the output mechanical power is given by both the gas turbine of the topping cycle and the steam turbine of the bottoming cycle. The air, suctioned by the external environment, is compressed by a centrifugal compressor and delivered into the high temperature gas to gas heat exchanger (HTHE), where it undergoes a great temperature increase. The air exiting the HTHE can expand through the gas turbine, which transforms the air enthalpy into mechanical work. After the expansion is concluded, the air discharged from the turbine is delivered into the combustion chamber, in which the combustion between the biomass and the oxygen present in the air takes place. The produced hot gases are conveyed firstly into a cleaning system (represented by an insulated cyclone separator) and then into the HTHE to transfer their heat to the compressed air (the latter is going to enter the turbine) without mixing with each other. After the heat exchange is concluded, the cooled down flue gases, rather than being exhausted into the atmosphere, are delivered to the heat recovery steam generator (HRSG) in order to generate superheated steam, which can expand through a small steam turbine. The steam can be expanded down to 1 bar (or similar pressure levels), rather than being expanded to lower pressures, in order to allow high temperature heat recovery (100 °C) from its condensation. In this way, the power plant is capable of producing useful thermal power in addition to electric power, thus achieving a combined heat and power configuration (CHP). Summarizing, the proposed architecture of combined cycles presents the following innovative aspects:

- The external combustor combined with the HTHE allows adapting gas turbine plants to dirty fuels: unlike internal combustion gas turbines (where the combustion gases enter the turbine), the combustion gases do not expand through the turbine, which is prevented from being damaged by metal and solid compounds generated by the combustion of dirty fuels, such as solid biomass.

- Different solutions can be adopted for the compressor-turbine group of the topping cycle. In fact, the compressor-turbine group can be taken from the automotive industry (since in several models the turbine blades are made of Nickel alloy and can withstand high temperatures, up to 1150 K) and coupled with a lower temperature power turbine (easy to manufacture). Alternatively, either an automotive compressor-turbine group can be adapted to be connected to an electric generator or a compressor-turbine-generator assembly can be manufactured ex-novo.
- The bottoming part of the power plant is a typical steam cycle, but with the particularity of having its components downsized in comparison with typical steam cycles employed for energy generation. The commercially available ‘’Green steam turbine’’ is proposed to be used as the micro-turbine of the bottoming cycle [11]; it is a cheap model that is capable of generating a maximum electrical power of about 15 kWe, with a maximum pressure of 10 bar and a maximum temperature of 225 °C. Using the data provided by the manufacturer, the isentropic efficiency can be estimated to be equal to about 50%, which is the highest value among commercially available micro-steam expanders.

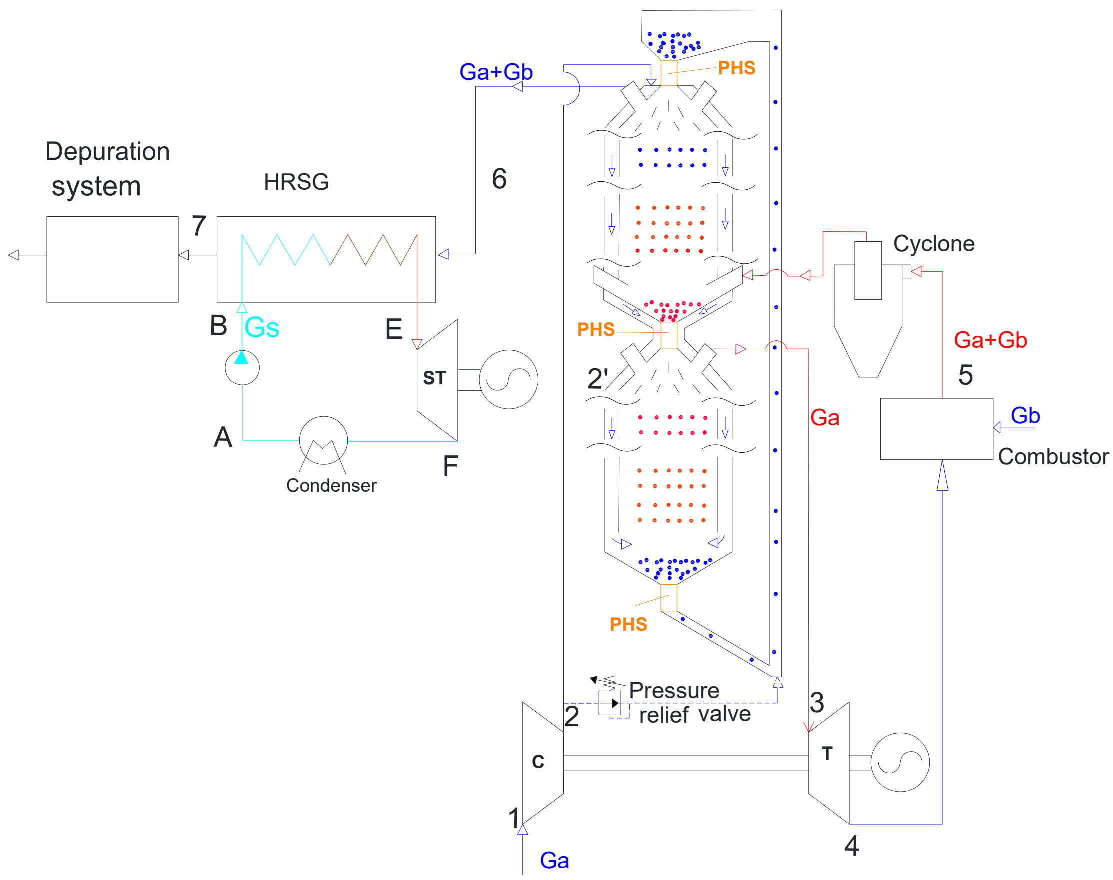

Fig.2. Application of the IPHE to small scale combined cycles (PHS= particle handling systems, HRSG=heat recovery steam generator, G_a= air mass flow rate, G_b= fuel mass flow rate, G_s=steam mass flow rate)

The IPHE serves as the HTHE and can be composed of either one or more modules, depending on the values of the mass flow rates. As shown in Fig. 1, each module is composed of two heat exchange columns: the upper one has the function of heating up small ceramic particles falling from its top down to its bottom, in counter-flow with the hot gases coming from the external combustor. The gases rise from the bottom of the upper column up to its top; afterwards, they leave the IPHE and enter the HRSG. Simultaneously, the warmed up particles exiting the upper column are collected, pressurized and transferred into the lower column; during their fall within the bottom column, they transfer heat to the compressed air coming from the compressor, increasing its temperature up to the level required by the gas turbine. In order to guarantee a continuous operation mode, the particles must be delivered back from the bottom to the top of the plant. This task is performed by a pneumatic conveyor, which uses a very small part of the compressed air to lift the particles up to the top of the heat exchanger. The pressure needed to lift the particles can be adjusted by using a pressure relief valve, as shown in Fig. 1.

Because of the pressure difference existing between the two columns (the upper one is almost at ambient pressure, whereas the lower one is at the same pressure as that generated by the compressor), three particle handling systems are introduced and designed in this work in order to effectively transfer the particles between the two columns. The upper handling system allows transferring the particles coming from the pneumatic conveyor into the upper column, the central system serves as a particle pressurization system needed to transfer the particles from the lower pressure environment into the higher-pressure one, whereas the lower system allows the particles to be moved from the lower column into the pneumatic conveyor. As shown in Fig. 1, each particle handling system is preceded by an accumulation reservoir, in order to enable the variation in the particle flow rate, thus giving high flexibility to the whole system.

Initially, the IPHE was thought to be employed in medium and large-scale power plants employing dirty fuels such as coal [22]; however, a more sustainable project is its application to small-scale power plants capable of burning biomass on site to produce useful heat power in addition to the electrical power. Furthermore, in the initial solution proposed for the IPHE [23], both columns were proposed to be realized in ceramic material, which can withstand the high temperatures present in a Joule Brayton cycle. However, this choice could lead to high investment costs and difficulties manufacturing the project idea. To overcome this issue, a new solution is developed in this paper: it consists in manufacturing every part of the IPHE out of steel, whose thermo-mechanical resistance can be ensured by cooling the walls. This can be achieved by letting the compressed air flow through the path shown in Fig. 1 before entering the lower column: in such a way, the compressed air can flow through the external channels surrounding the most critical parts of the IPHE (walls of the columns as well as pressurization system), thus taking heat away from the walls of the IPHE. A similar strategy is used in both heavy duty and aero derivative gas turbines, in which a part of the compressed air (referred to as secondary air) is used to cool the combustor liner and prevent the metals of the combustor from being damaged.

2.2 Architecture and analytical model proposed for the particle handling systems

As mentioned before, because of the different pressure levels existing between the two columns, adequate systems must be designed to move the particles within the IPHE. The authors dealt with this task also in previous papers [22]; the previous work has allowed conceiving the solution presented in this paper. Fig. 2 shows the solution proposed for the three particle handling systems: each of them is made up of a convergent reservoir, a guillotine valve and a rotary valve. With regard to the latter, it is a component widely used in several industrial fields, allowing particles and loose material to be moved from two environments at different pressures. It is mainly composed of a gear rotor rotating within a cover interposed between two environments at different pressure. A few commercially available solutions have been recently proposed to avoid the interference occurring among the particles, the moving parts and the stator. One of these employs helical profiles for the blades of the rotor, another employs particular shapes for the inlet section; either one could be used in the present case, thus avoiding interference problems noticed in previous studies [23].

The application of these systems to the IPHE can be made possible by using a reservoir to be placed downstream of the rotary valve, in addition to a guillotine valve to be interposed between the rotary valve and the reservoir. In this way, the adjustment of the opening degree of the guillotine valve can allow the quantity of particles entering the rotary valve to be regulated properly, thus avoiding particle accumulation at the inlet of the rotary valve, which could result in interference issues. With this system, the particle flow rate injected into the columns can be adjusted by acting on the rotational speed of the rotors, while the opening degree of the guillotine valves can be changed to ensure the highest possible filling within the rotor chambers while avoiding particle interference.

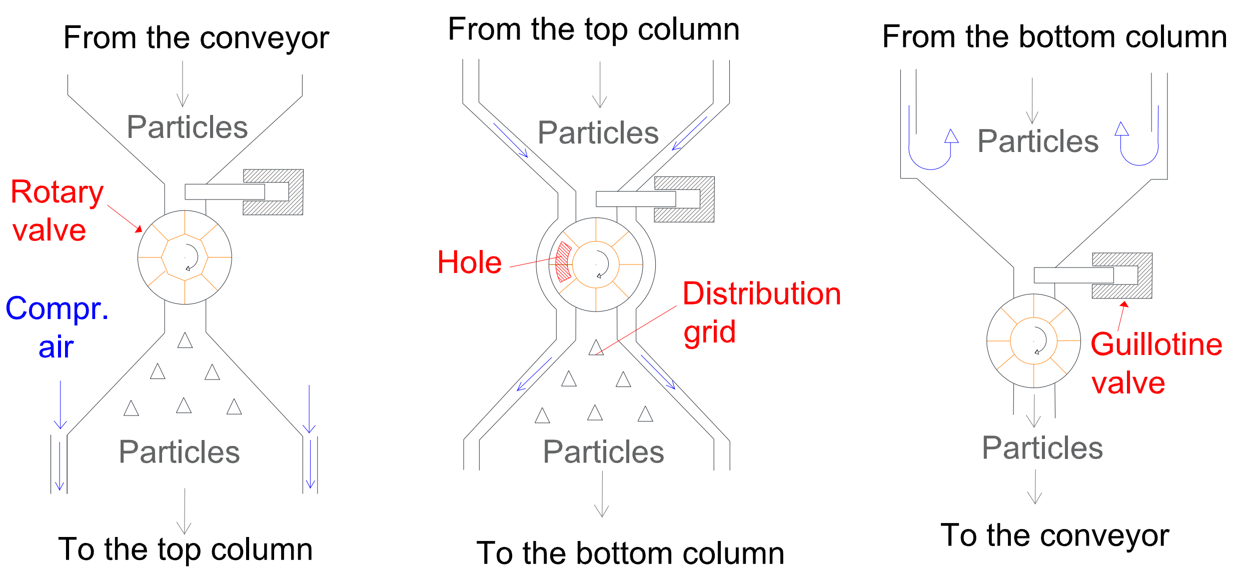

Fig.2. Configuration proposed for the particle handling systems (left: upper system, centre: pressurization system; right: lower system)

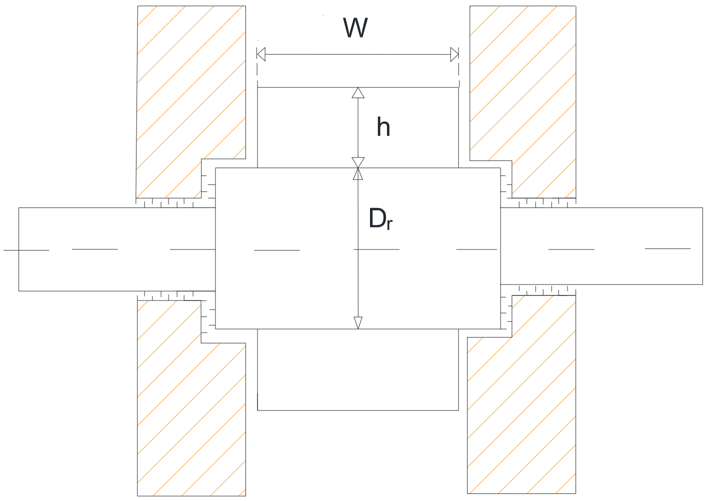

Fig.3. Geometric parameters of the three rotary valves (W=blade width; h=blade height; D_r=rotor diameter)

Another innovative aspect presented in this paper regards the materials to be used for manufacturing the particle handling systems: in fact, in the new architecture proposed, all the three systems can be made out of stainless steel, even the central one. The latter is the most critical, because it operates at the highest temperatures; however, the external cooling system (achieved by means of the internal channel for the compressed air, see Fig. 1 and 2) can allow steel to withstand such critical conditions without having to make the rotor and its blades out of more expensive ceramic materials. The only precautionary measure to be taken for the central rotary valve can be to coat its steel blades and the steel rotor surface with a layer of ceramic material (e.g. alumina), in order to enhance the thermo-mechanical resistance of the surfaces in contact with the hot particles.

Unlike the top and bottom rotary valves, the central one presents a hole in its cover, which is connected with the top column by means of an additional pipe. This solution is needed to facilitate the passage of the particles from the top column into the chamber of the rotor. In fact, after the particles have been discharged from a rotor chamber into the bottom column, the chamber is full of compressed air, which needs to be ejected from the chamber in order to lower the pressure to the atmospheric value and attain the same pressure as that of the top column, thus allowing the particles to enter the rotary valve more effectively. The air ejected from the hole is recovered by means of the above-mentioned pipe and delivered into the top column.

The particles must be introduced at the top of each column as uniformly as possible over the entire diametral section of the column, in order to maximize the heat exchange with the counter-flowing gas (which is combustion gas in the top column and compressed air in the bottom one). For this reason, a distribution grid is placed downstream of the rotary valve in both columns in order to distribute the particles over the entire flow area.

The volume of each rotary valve can be calculated by using the following equation:

$$G_p = \lambda_v \, \rho_p \, V \, n \, n_{mod} \tag{1}$$

where G_p is the overall particle mass flow rate, λ_v is the filling coefficient (which takes into account the real volume occupied by the particles within the rotor chamber), ρ_p is the particle density, *V* is the volume of the particles discharged per revolution, *n* is the rotational speed and n_{mod} is the number of modules the IPHE is split into. Using the symbols shown in Fig. 3, the volume calculated through equation (1) can be related to the width (*W*) and height (*h*) of the blades as follows:

$$V = \xi W h (D_r + h) \pi \tag{2}$$

where ξ is a coefficient taking into account the blade thickness and D_r is the diameter of the rotor. In order to achieve an optimum filling, the width of the blades (*W*) should be taken large, whereas their height (*h*) and the diameter of the rotor (D_r) should both be taken small. As an example, having adopted the geometric relations h=W/2 and D_r=W, equation 2 becomes equation (3) allowing the width of the blades (W) to be calculated:

$$V = \xi \frac{3W^3}{4} \pi \tag{3}$$

The implementation of the three particle handling systems along with the pneumatic conveyor causes a small quantity of compressed air to move from the bottom column into the top one. This compressed air escaping the bottom column does not move to the external environment but enters the top column, thus being useful for the bottoming cycle. However, this must be considered as a loss of compressed air, because such a small quantity of compressed air cannot expand through the gas turbine. The total loss of compressed air $G_{a,lost}$ is the sum of the following contributions:

1) Quantity of compressed air ($G_{a,lost,1}$) moving from the bottom column to the top one because of the pressurization system (central rotary valve). This loss is due to the fact that, after the particles have been discharged from a chamber (volume comprised between two blades) of the rotary valve into the bottom column, the chamber is full of compressed air. This air needs to be ejected from the chamber in order to lower the pressure to the atmospheric value; this is achieved by means of a pipe connecting the top column with the rotor. This loss can be calculated as follows:

$$G_{a,lost,1} = \rho_3 \, V n \, n_{mod} \tag{4}$$

where ρ_3 is the density of the compressed air at the outlet of the bottom column.

2) Quantity of compressed air ($G_{a,lost,2}$) moving from the bottom column to the pneumatic conveyor because of the bottom rotary valve. This loss is due to the fact that a small quantity of compressed air occupies the interstices comprised among the particles within the rotary valve during the particle

transfer from the bottom column into the pneumatic conveyor; as a result, this compressed is transferred into the pneumatic conveyor together with the particles. This loss can be calculated as follows:

$$G_{a,lost,2}=(1-\lambda_v)\rho_{2'}\,Vn\,n_{mod} \tag{5}$$

where $\rho_{2'}$ is the density of the compressed air at the inlet of the bottom column.

3) Quantity of compressed air ($G_{a,lost,3}$) taken from the compressor to lift the particles from the bottom to the top of the plant. In this regard, it must be considered that the power required to lift the particles (equal to $G_p\ g\ H$, where g is the gravitational acceleration and *H* is the total eight of the IPHE) multiplied by the efficiency of the pneumatic conveyor η_{conv} must equal the mechanical power taken off the gas turbine. By equating these two quantities, one obtains the air mass flow required by the pneumatic conveyor:

$$G_{a,lost,3}=\frac{G_p\ g\ H}{(i_3-i_4)\eta_{conv}} \tag{6}$$

This analysis has neglected the loss of compressed air that passes between the blade of the rotor and the cover and that moves from the bottom column to the top column. This further loss can be neglected for two reasons, both due to the use of metallic material (steel). The first reason is that the employment of metallic material allows the clearance between the inner diameter of the case and the rotor blade to be reduced as much as possible. In addition, the use of metallic material allows an easy and effective design of air tight systems (Fig. 3 shows an air tight system achieved with labyrinth seals which prevent air leakage to the external environment).

2.3 Architecture and analytical modelling of the top and bottom columns

The architecture conceived in this paper for both columns is different from that presented in previous studies [24]; in the new solution presented here, the compressed air coming from the compressor is delivered to the top of the IPHE, from which it flows downwards within an internal channel comprised between the external casing and the walls of the columns. During this path, the compressed air cools the walls of the IPHE until reaching the inlet of the bottom column; at this point, the compressed air inverts its direction and flows upwards and is heated by the particles until it reaches the outlet of the bottom column (which is connected to the gas turbine). Contemporaneously, the hot gases enter the top column and heat the particles up during their upward motion.

This new solution has been introduced because it has the potential not only to dramatically reduce the capital costs (by avoiding using ceramic and/or composite materials) but also to minimize the thermal dispersion towards the external environment. The latter feature can further be enhanced by insulating the external casing of the heat exchanger.

The diameters and heights of both columns as well as the particle diameter and the particle flow rate must be chosen properly to achieve the desired heat exchange efficiency of the IPHE, η_{IPHE} , which can be defined as follows (see Fig. 1 for symbols):

$$\eta_{IPHE} = \frac{i_3 - i_2}{i_5 - i_2} \quad (7)$$

In the top column, the thermal power released by the hot gases is acquired mainly by the particles and partially by the compressed air. This heat transfer in the top column can be expressed as follows (see Fig. 2 for symbols):

$$(G_a + G_b)(i_5 - i_6) = G_p(i_{p,top} - i_{p,press}) + G_a(i_{2'} - i_2) \quad (8)$$

where $i_{p,top}$ and $i_{p,press}$ are the enthalpies of the particles at the top and bottom of the top column, respectively; $i_{2'}$ denotes the enthalpy of the compressed air exiting the external channel of the top column. In the bottom column, the heat transfer between the particles and the compressed air is given by equation 9:

$$G_a(i_3 - i_{2'}) = G_p(i_{p,press} - i_{p,bottom}) \quad (9)$$

where $i_{p,bottom}$ denotes the enthalpy of the particles exiting the bottom column. The latter can be related to the enthalpy of the particles entering the top column, $i_{p,top}$, as follows:

$$i_{p,top} = i_{p,bottom} - \Delta i_{p,loss} \quad (10)$$

where $\Delta i_{p,loss}$ represents the enthalpy that the particles lose during their rise from the bottom to the top of the plant. It is crucial to design the bottom and top particle handling systems as well as the pneumatic conveyor so that $\Delta i_{p,loss}$~ 0. To accomplish this, these systems must be insulated properly; and this is a simple task because the particles moving from the bottom to the top of the plant have a low temperature, which is expected to be slightly higher than the temperature of the air exiting the compressor (T_2). In addition, the heat exchange between the particles and the air can be neglected in the conveyor, because the quantity of air mass flow rate taken by the pneumatic conveyor is very small and has a temperature level very similar to that of the particles exiting the bottom column (the air is taken from the compressor outlet at the temperature T_2).

2.4 Computational fluid dynamics modelling of the top and bottom columns

By virtue of the symmetry of the geometry, and in order to reduce the computational time, only a quarter of the fluid domain can be meshed for both columns by using the software Ansys Fluent [25].

Fig. 4 shows the whole architecture of the top column and the part of the top column that was simulated, namely only the part needed for the heat exchange between the particles and the counter flowing gas. The distribution grid at the top of the column must be designed so as to distribute the particles over the entire flow section; similarly, the inlet ducts for the combustion gases are to be designed so as not to distort the gases ascending the top column, in addition to ensuring negligible pressure drops. The CFD analysis was therefore conducted only on the part of the top column responsible for the heat exchange with the hypothesis that both the particles are injected over the entire flow area and the hot gases enter this part of the column uniformly. In this manner, it was possible to let the optimization procedure effectively find out the values of the diameter and height of the top column (D_{top} and H_{top}) that are necessary to achieve the desired heat exchange. After the diameters and heights have been found by the optimization procedure, it will be possible to correctly design both the particle distribution grid and the inlet ducts in order to achieve the above-discussed features. This will be the objective of forthcoming studies. Fig. 5 shows the structured grid generated for the top column along with the zone types employed, which are also visible in Fig. 4 for ease of comprehension. The two fluids, namely the compressed air and combustion gases, are counter-flowing and are separated by a solid domain, which is meshed with hexahedral elements. The combustion gases enter the internal domain through *Inlet 1* and exit the internal domain through *Outlet 1*; simultaneously, the compressed air enters the external domain through *Inlet 2* and exits the external domain through *Outlet 2*.

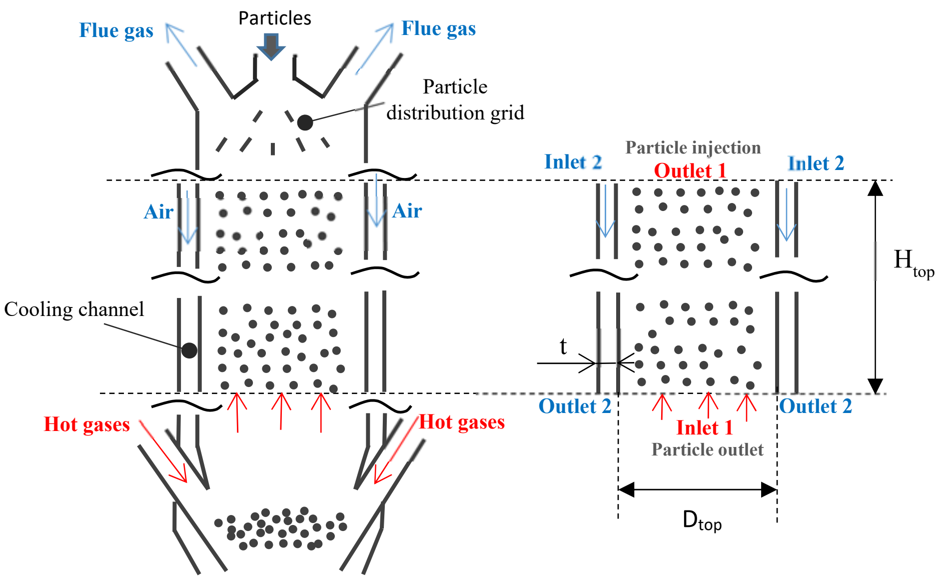

Figure 4. Architecture for the top column (left) and simulated part (right)

(design parameters: H_{top} and D_{top}; fixed parameter: t=0.06m)

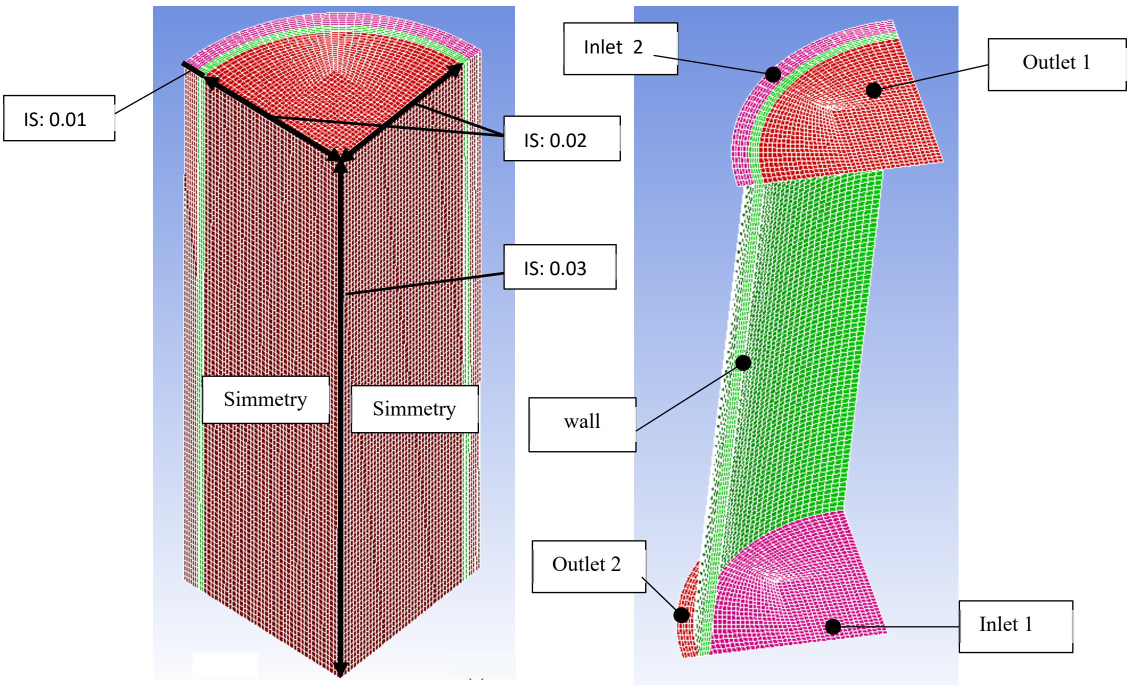

Fig. 5. Computational grid employed for the top column, example for D_{top}=1.5 m and H_{top}=3m.
(IS=interval size expressed in meters)

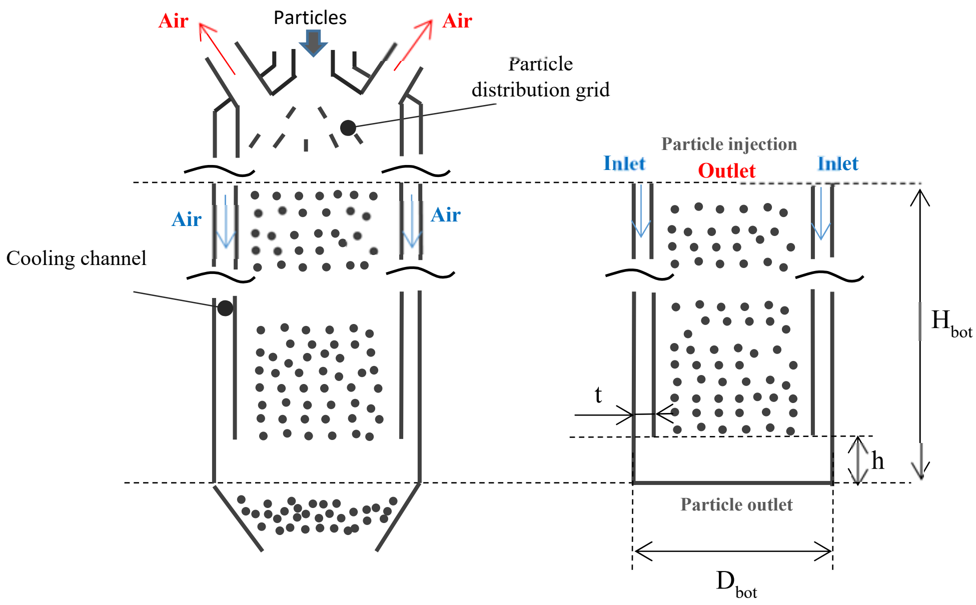

Fig. 6. Architecture for the bottom column (left) and simulated part (right)

(design parameters: H_{bot} and D_{bot}; fixed parameters: t=0.06m and h=0.3m)

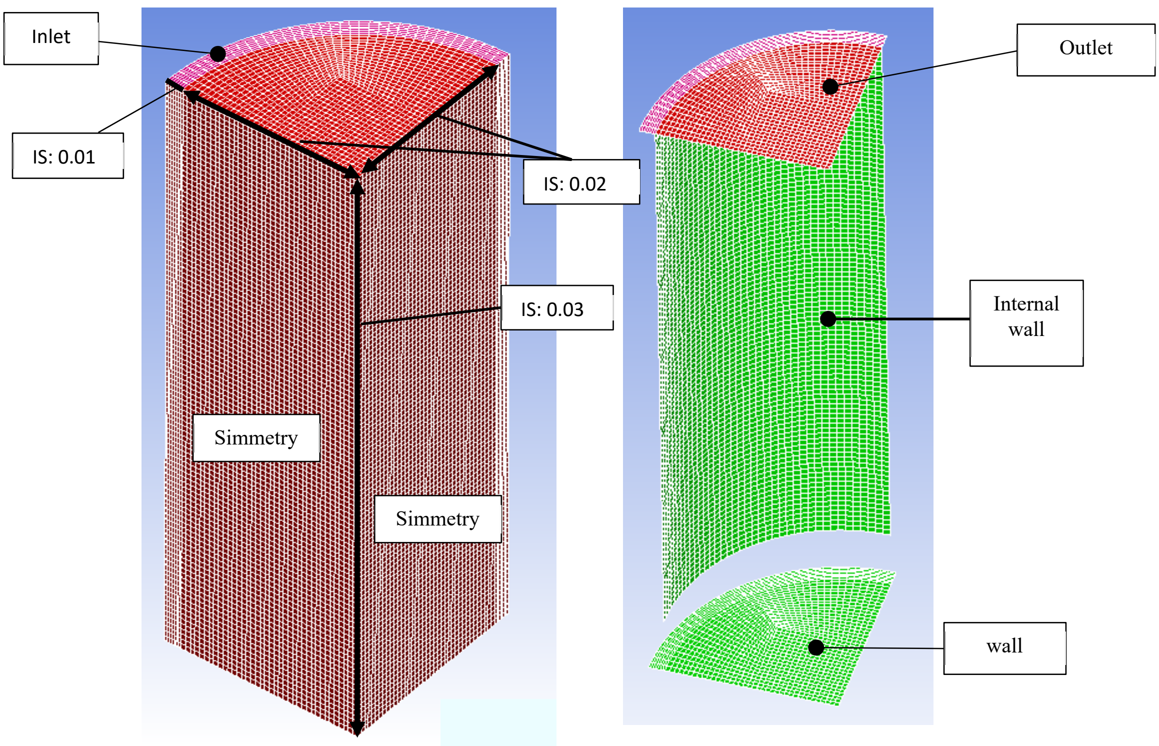

Fig. 7. Computational grid employed for the bottom column; example for D_{top}=1.5 m and H_{top}=3m

(IS=interval size expressed in meters)

Similarly, Fig. 6 shows the whole architecture of the bottom column and the simulated part. Also in this case, the zone associated with the distribution grid was not simulated, as the aim of this work is to find the dimensions (height and diameter) of the part necessary to achieve the desired heat exchange for both columns. Fig. 7 shows the computational grid generated for the bottom top column along with the zone types employed (which can also be seen in Fig. 6). The compressed air enters the external domain through the *Inlet* and flows through the external channel comprised between the inner and the outer walls. After having entered the bottom column through an internal section, the air flows upwards and exits the domain through the *Outlet*. In this case, the wall separating the external channel from the internal part of the column is not meshed; instead, an internal surface is used and defined as an internal wall with a specified thickness. This strategy is used to avoid meshing a very thin solid domain (in the bottom column, the wall separating the flux of descending air from the flux of ascending air can be designed very thin because the two fluxes have the same pressure).

For both mesh typologies, the two surfaces where the physical geometry and the flow pattern have mirror symmetry are defined as symmetry zones.

With regard to the mesh setting employed in the optimization process, the strategy was to mesh fixed edges with fixed interval sizes, as shown in Fig. 4 and Fig. 6. The remaining edges were meshed with an interval size necessary to achieve a structured grid in the entire domain. With this setting, the size of the computational grid (number of cells) depends on the values of the dimensions (e.g., the computational grids reported in Fig. 5 and Fig. 7 have a size of about 150000 cells), but the simulation of the fluid is very similar for all the geometries explored by the optimizer regardless of their dimensions, because the interval size is the same for the selected edges. The fixed values of the interval sizes results from a grid independence analysis, not reported here for brevity; the maximum skewness factor is less than 0.5 for all meshes.

Table 1 reports the boundary conditions associated with the zone types shown in Figures 5 and 6. The particles in the top and bottom columns are injected, with imposed mass flow rate and temperature, from *Outlet 1* (fig. 5) and *Outlet* (fig.7), respectively; the injected particles are allowed to exit through *Inlet 1* (fig.5) and the bottom *Wall* (fig. 7). The main properties of both the continuous phase and the particles are reported in Table 2. The combustion gas properties were assumed equal to the compressed air properties for simplicity; the conduction inside the particles is neglected because of their small size.

The discrete phase model is employed: it is able to solve transport equations for the continuous phase (compressed air or combustion gases), and to simulate the discrete second phase (ceramic particles) in a Lagrangian frame of reference. Fluent computes the trajectories of these discrete phase entities, as well as heat and mass transfer to/from them. The coupling between the phases calculates the impact both on the discrete phase trajectories and on the continuous phase flow. The trajectory is based on the force balance on the particle (gravity and drag in the present case), while heat transfer calculations are based on the convective and radiative heat to/from the particle, using the local continuous phase conditions as the particle moves through the flow.

The standard k-ω model is employed to predict turbulence. This model was selected as it shows high performance for wall-bounded flows, providing high accuracy [25]. Furthermore, it is very suitable for optimization processes (in which the conditions near walls remarkably change from solution to solution) allowing for a very accurate near wall treatment with an automatic switch from a wall function approach to a low-Reynolds number formulation according to the values of y+ [25].

All the equations are solved using second order discretization schemes. With regard to the number of iterations, about 2000 iterations are needed to reach a very good converge level (less than 10^{-4} in all the scaled residuals, with the energy residual being of the order of 10^{-6}). As no data are available in the scientific literature (this architecture is new), the confidence in the CFD model was established by analysing the residual levels for the energy (which is of the same order as the software default convergence criterion) and by checking the predicted heat transfer between gas and particles. In fact, using larger interval sizes than those shown in fig. 5 and fig. 7, the simulations provided inaccurate results in terms of heat exchange: in such a case, the predicted amount of heat flow that was released from the hot particles was different from the one transferred to the cold air in the bottom column (the same happened for the top column).

Column	Zone type	Boundary condition	Values
Top column	Inlet 1	Mass flow inlet	Mass flow rate= $\frac{G_a+G_b}{4\ \mathrm{n_{mod}}}$ Temperature= T_5
	Outlet 1	Pressure outlet	Pressure= p_6
	Outlet 1	Particle Injection	Particle flow rate= $\frac{G_p}{4\ \mathrm{n_{mod}}}$ Particle temperature= $T_{p,top}$
	Inlet 2	Mass flow inlet	Mass flow rate= $\frac{G_a}{4\ \mathrm{n_{mod}}}$ Temperature= T_2
	Outlet 2	Pressure outlet	Pressure= p_6
Bottom column	Inlet	Mass flow inlet	Mass flow rate= $\frac{G_a}{4\ \mathrm{n_{mod}}}$ Temperature= $T_{2'}$

	Outlet	Outflow	
	Outlet	Particle Injection	Particle flow rate=$\frac{G_p}{4\,\mathrm{n_{mod}}}$ Particle temperature=$T_{p,press}$

Table 1. Zone types and boundary conditions employed for both columns (see Fig.1 and Fig.2 for symbols; n_{mod} denotes the number of modules the IPHE is split into)

Phase	Density (ρ)	c_p [kJ/kgK] (specific heat)	λ [W/mK] (Thermal conductivity)
Fluid	Incompressible ideal gas	$c_p = \frac{1}{M}(a+bT+cT^2+dT^3)$[26] a=28.11 b=0.1967*$10^{-2}$ c=0.4802*10^{-5} d=-1.966*10^{-9} M=28.97 kg/kmol; T in K	$\lambda = a+bT+cT^2$ [26] a=0.003782 b=7.948*10^{-5} c=-1.610*10^{-8} T in K
Particles	3600 kg/m^3	$c_p = a+bT+cT^2+dT^3$ [26] a=175.7 b=2.8085 c=2.5814*10^{-3} d=8.268*10^{-7} T in K	Particle conduction is neglected
Internal walls	Solid (steel)	502.48 J/(kgK)	16.27 W/(mK)

Table 2. Properties set for the fluid, particles and the internal walls

2.5 Optimization process

In order to accomplish the task of designing both columns so as to achieve the desired heat exchange efficiency η_{IPHE}, an optimization process design is proposed that is based on the coupling between a genetic algorithm and a CFD analysis of the heat exchange between the particles and the gas within both columns. The optimization design consists in a sequential and iterative process implemented in the optimization software ModeFRONTIER [27]. With regard to the optimization algorithm, MOGAII was chosen as the optimizer; the efficiency of the employed algorithm is due to the new "directional cross-over" operator, which outperforms the classical "two point cross-over" [28]. The parameters chosen for MOGA II are shown in table 3: the effectiveness of this setting was demonstrated in previous studies [29].

Parameter	Value
Probability of directional cross over	0.5

Probability of Selection	0.05
Probability of Mutation	0.1
Elitism	enabled

Table 3 .Parameters of MOGA II

The initial population was generated by the employed DOE algorithm (Constraint Satisfaction, with a number of individuals equal to 100, which corresponds to the number of individuals per generation).

The chosen design parameters are: number of heat exchangers (n_{mod}), height (H_{top}) and diameter (D_{top}) of the top column, height (H_{bot}) and diameter (D_{bot}) of the bottom column, particle diameter (D_p). The first design parameter, namely the number of heat exchangers (n_{mod}), is introduced to explore the possibility of splitting the IPHE into more modules, with each module being composed of a top column coupled with a bottom column. In the optimization procedure, this parameter determines how many parts the gas flow rate (G_a+G_b), the air flow rate (G_a) and the particle flow rate (G_p) must be split into. Therefore, according to the value of n_{mod}, the boundary conditions are calculated as shown in Table 1. To avoid the generation of large but short columns, the constraints $H_{top}>D_{top}$ and $H_{bot}>D_{bot}$ were imposed. With regard to the value assumed for the particle flow rate G_p, it was fixed equal to the values of the gas flow rate G_a+ G_b, in order to reduce the number of design parameters.

The objectives are the minimization of the overall heat exchange surface S_{tot} and the minimization of the difference $\left|T_{3,sim} - T_3\right|$, where $T_{3,sim}$ is the predicted temperature of the air exiting the bottom column and T_3 is the desired fixed inlet temperature of the gas turbine. The minimization of the overall heat exchange surface was chosen as objective because it is important to design the heat exchanger as compact as possible: the bulkier the heat exchanger, the more expensive the overall cost. Furthermore, the implementation of a very large heat exchanger would be unfeasible for such a small scale power plant. The large surfaces needed for the heat exchange is a common problem of typical gas to gas heat exchangers, therefore this objective allows understanding whether the novel architecture of the IPHE can effectively overcome this issue. The second objective was chosen because the IPHE must provide a desired heat exchange efficiency and hence a desired inlet temperature of the gas turbine.

The design parameters, objectives and constraints are summarized in Table 4 for completeness.

The evaluation of the individuals is automatically performed through the following procedures:

(a) CFD simulation of the top column, which leads to the calculation of the predicted temperature of the particles exiting the top column, $T_{p,press, sim}$.

(b) CFD simulation of the bottom column, aimed at the calculation of the air temperature at the outlet of the bottom column, $T_{3,sim}$.

(c) Evaluation of the objectives, selection, crossover and mutation .

Design parameters	n_{mod}, H_{top}, D_{top}, H_{bot}, D_{bot}, D_p
Objectives	Minimization of both S_{tot} and $\left\|T_{3,sim} - T_3\right\|$
Constraints	$H_{top} > D_{top}$, $H_{bot} > D_{bot}$ $\left\|T_{p_{press},sim} - T_{p,press}\right\| < \varepsilon_{tol.}$
Fixed parameters	$G_p = G_a + G_b$ T_2, T_3, T_5, G_a, G_b, $T_{p,press}$, $T_{p,top}$, η_{IPHE}

Table 4. Design parameters, objectives, constraints and fixed parameters (see fig.1 for symbols)

In order to speed up the entire optimization procedure, the passage from step a (CFD simulation of the top column) to step b (CFD simulation of the bottom) column is allowed only if all the particles can fall down and if the predicted particle temperature at the exit of the top column ($T_{p,press,sim}$) reaches the desired value at the exit of the top column, namely $T_{p,press}$ (a tolerance coefficient ε_{tol} can be introduced, as shown in Table 4). The latter value ($T_{p,press}$) is a fixed parameter and can be determined, for a given heat exchange efficiency of the IPHE (η_{IPHE}), by using equations 7-10, which can allow fixing the particle temperatures both at the outlet of the top column ($T_{p,press}$) and at the inlet of the top column ($T_{p,top}$). Summarizing, the value of $T_{p,top}$ must be used, in the CFD simulation of the top column, as the injection temperature of the particles into the top column. In contrast, the value of $T_{p,press}$ must be used as the temperature to reach through step a (CFD simulation of the top column), which enables the activation of step b (CFD simulation of the bottom column). A flow chart of the optimization process is reported in Fig. 8.

The CFD simulations of the columns represent a great part of the computational cost of the entire procedure, while the optimization process presented here needs to be compatible with typical industrial design time. To address this issue, the computational grid partition together with the parallel processing was employed to reduce the overall processing time. The grid partitioning, or domain decomposition, consists in splitting the computational grid of a single individual into smaller sized grids that allow the contemporary use of more than one processor of the same machine. Such a decomposition speeds up the computation since it fits within the memory limits of the employed machine. In addition, the parallel processing allows the concurrent evaluation of more individuals, and this tool is not available for gradient based algorithms or similar ones, e.g. the Simplex algorithm, which cannot afford multiple evaluations to make decisions. In contrast, a genetic algorithm makes decisions and generates a new population of individuals only after the entire current population has been explored, thus fitting the parallel processing very well.

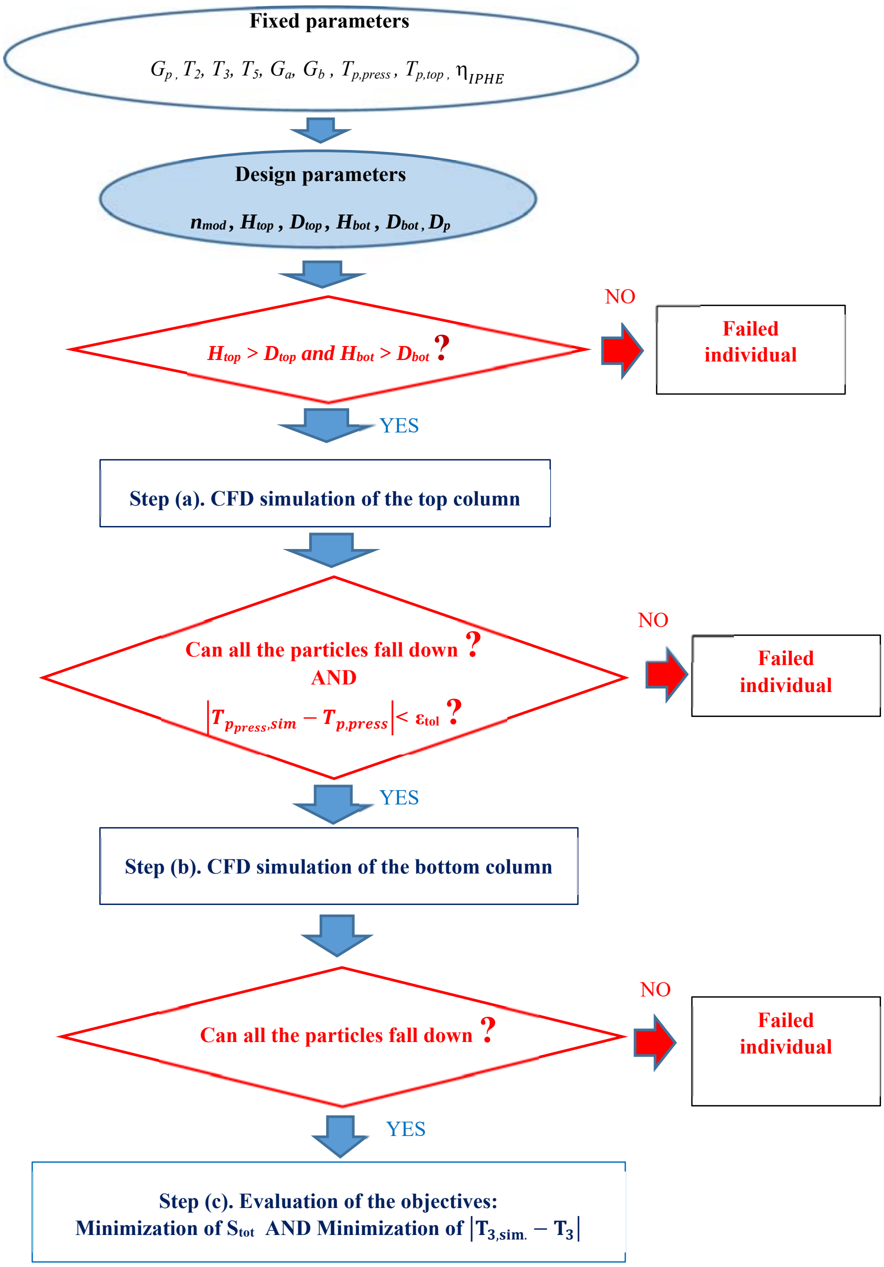

Fig.8- Flow chart of the optimization process (see Fig.1 for symbols)

3. Results

The geometric optimization procedure was applied to the small scale combined cycle (see Fig.1) characterized by the thermodynamic values reported in [11] and obtained through the thermodynamic optimization procedure presented in [11]. The study performed in [11] was instrumental in determining the values of the cycle parameters (temperatures and flow rates) that allowed the plant performances to be optimized. Different objective functions were considered, namely the optimization of the electrical efficiency of the combined cycle, the optimization of the thermal efficiency of the combined cycle and the optimization of the overall efficiency of the combined cycle. In this work, the methodology presented in Section 2 is applied to the latter case (optimization of the overall efficiency of the combined cycle). Fig. 9 reports the corresponding values of the thermal parameters and flow rates, namely those parameters that allow the overall efficiency of the combined cycle (electrical efficiency plus thermal efficiency) to be optimized. In these conditions the heat exchange efficiency required to the IPHE , η_{IPHE} (expressed through equation 7), is equal to 0.75. As discussed in [11], the heat exchange efficiency was set to this value so as to increase the temperature of the flue gases entering the HRSG (T_6) and hence to maximize the thermal power transferred in the HRSG, allowing a great quantity of thermal and electrical energy to be generated in the bottoming cycle.

The electrical efficiency of the power plan is 0.2212 according to the calculation performed in [11]. This value was determined assuming that the pressure drops in the part of the circuit from the gas turbine exit to the HRSG exit are negligible. This assumption was thoroughly discussed and justified in [11], where each component was analysed in detail. The pressure drops in the HRSG and cyclone separators [29] are usually so low that they can be neglected for the calculation of thermodynamic properties. The IPHE, serving as the HTHE, produces negligible pressure drops either, and this assumption will be verified in the following. The most critical component in terms of pressure drops is usually the combustor; however, it should be noted that, in the present configuration, it operates at ambient pressure and therefore can be designed more effectively than typical pressurized fluidized bed combustor. In addition, the design of the components in the present plant can take advantages of the very low air flow rate of the circuit in order to minimize the pressure losses.

In case of non-negligible pressure drops in line 4-7 (see fig.1 and fig.9), a fan would be needed at the exit of the HRSG in order to compensate for these losses. The absorbed power would penalize the net electrical power and hence the efficiency of the plant. Figure 10 shows a graph reporting how the performance of the plant would be penalized by the increasing pressure drop in line 4-7, which evidences the importance of minimizing the pressure drops. According to this calculation, if the pressure drops are maintained within the order of 0.05 Pa, then the electrical efficiency will be reduced by 1% only.

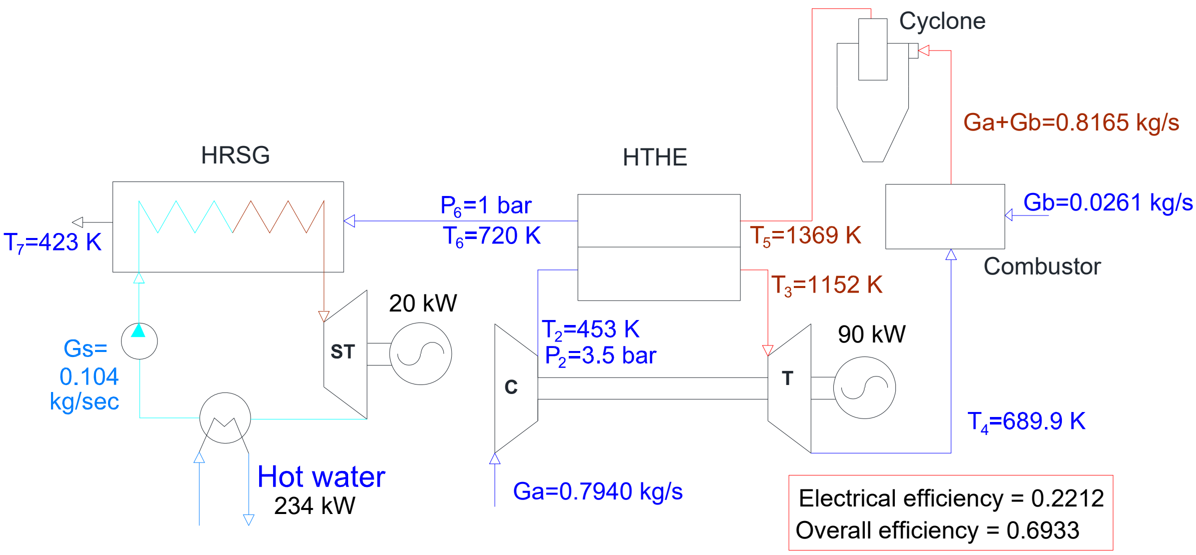

Fig. 9. Case of study for the application of the IPHE

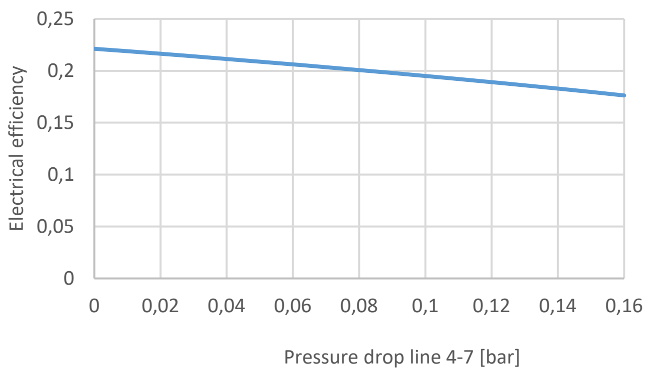

Fig. 10. Electrical efficiency (net electrical power over input thermal power) as a function of the pressure drop in line 4-7

The chosen design space is reported in Table 5; Table 6 reports the values of some thermal parameters fixed in the optimization procedure. As mentioned earlier, the values of both $T_{p,top}$ and $T_{p,press}$ were determined by using equations 7-10. The explanation for these fixed values was exposed in Section 2 thoroughly. Table 6 reports some geometrical parameters fixed for both columns.

Design parameter	Unit	Range	Step	Number of points
number of heat exchangers (n_{mod})	/	1-6	1	6
height of the top column (H_{top})	[m]	0.4-3	0.1	27
diameter of the top column (D_{top})	[m]	0.3-2	0.1	18
height of the bottom column (H_{bot})	[m]	0.4-3	0.1	27

diameter of the bottom column (D_{bot})	[m]	0.3-2	0.1	18
particle diameter (D_p)	[mm]	0.1-1	0.01	91

Table 5. Design space employed in the optimization procedure

Parameter	value
G_p (kg/sec)	0.8165
$T_{p,top}$ (K)	620
$T_{p,press}$ (K)	1220 (tolerance ε_{tol}= 10 K)

Table 6. Values assumed in the optimization procedure

Fixed geometrical parameters	value
Width of the external channel [m]	0.06
Width of the internal walls [m]	0.04
Roughness of the walls [m]	$5e^{-05}$
Reflection coefficient (interaction particle-wall)	0.5

Table 7. Geometrical parameters fixed for both columns

The process was stopped after 3000 individuals had been explored (termination criterion). The optimization process was managed by a personal computer equipped with an Intel core i7 processor at 3.3 GHz and 64 GByte of ram. Four configurations were computed in parallel and each configuration was partitioned into two sub-domains. With this hardware resource, and thanks to the strategy described in Section 2.4, two weeks were needed to conclude the optimization.

Fig. 11 reports two geometries explored for the top column by the optimization process. The first geometry (Fig. 11a) is characterized by an internal diameter very small (D_{top}=0.8m) but a considerable height (H_{top}=2.3 m), with the particle diameter being equal to D_p=0.26mm. In contrast, the second geometry (Fig.11b) is larger (D_{top}=1.2m) but shorter (H_{top}=1.8 m), with a particle diameter of D_p =0.6 mm. Both the particle contours and the gas velocity contours reveal that, in the first case, the particles are pushed against the walls and a part of them cannot fall down. This is due to the fact that the particle diameter is too small in comparison with the air velocity, with the latter being very high because of the small column diameter. As a result, the gas and the particles are confined in two different regions of the pipe, flowing separately. This behaviour must be avoided; in contrast, to achieve a correct operation of the IPHE and thus a high heat transfer efficiency, the particles must be distributed as uniformly as possible in all transversal sections; namely, the particle trajectories must be straight too. In the second case, the ratio of the particular diameter to the column diameter is more convenient and both the particles and the gas can flow more uniformly within the column.

However, in the latter case the final temperature of the particles is not high as expected, which means that the combination of design parameters is not optimal.

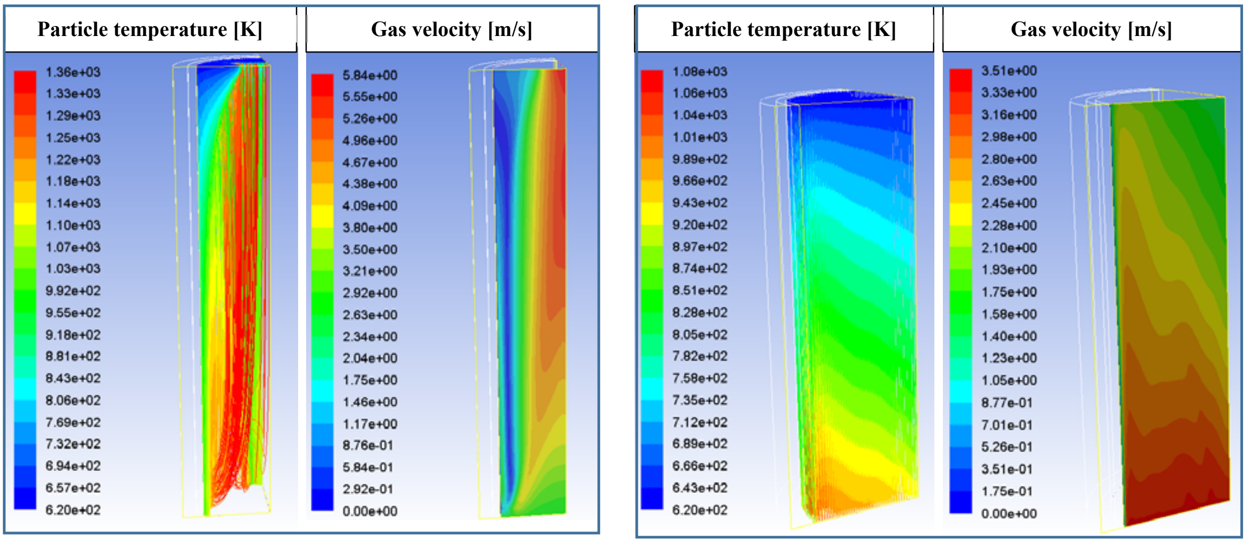

(a) (b)

Fig. 11. Non-optimal geometries for the top column. D_{top}*=0.8m,* H_{top}*=2.3m and* D_p*=0.26mm (a);* D_{top}*=1.2m,* H_{top}*=1.8m and* D_p*=0. 6mm (b)*

This comparison serves as an example to evidence that the particle diameter along with all the other geometric parameters must be properly selected in order to avoid that the gas flow distort the particle fall, pushing the particles away from a straight path (or vice-versa). The optimization procedure allows discovering and discarding the ineffective geometries, thus moving towards optimal solutions.

The optimization process allowed the determination of the Pareto Front, which represents the set of those individuals that are not dominated by any others; in other words, the Pareto Front represents the limit beyond which the design cannot further be improved. Figure 12 shows each feasible individual (combination of the design parameters that respect the prescribed constraints) plotted as a point at the location specified by its values of the objectives, namely S_{tot} and $|T_{3,sim} - T_3|$. Because of the imposed constraints, the number of feasible individuals results very small. It is possible to observe the Pareto Front located at the frontier of the feasible individuals; as expected, it is not possible to choose an individual belonging to the front that is capable of minimizing S_{tot} and minimizing $|T_{3,sim} - T_3|$ at the same time, because these objectives are conflicting; as a result, the optimum must be chosen according to which of the two performance parameters must be favoured and to what extent.

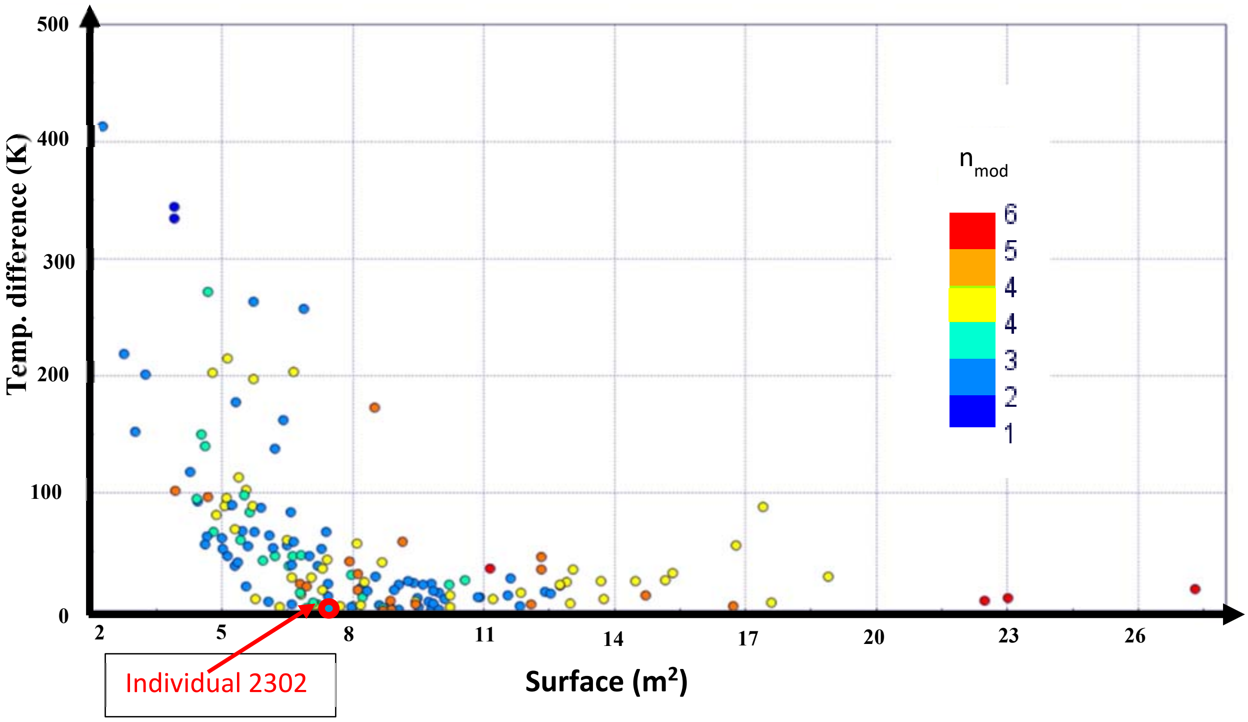

Fig. 12. Feasible individuals plotted in the objective space, with indictaion of the individual selected (individual 2302)

In this analysis, the minimization of $\left|T_{3,sim} - T_3\right|$ was preferred over the minimization of S_{tot}, because a reduction in T_3 would cause a consequential reduction in the efficiency of the cycle (see fig.9). According to this strategy, the optimum was selected among the non-dominated solutions of the Pareto front characterized by $\left|T_{3,sim} - T_3\right|$ being less than 0.5%. Among these, individual 2302 was selected because it has the lowest surface S_{tot} ; its values of the design parameters are reported in Table 8 along with the values of the objectives and constraints.

Individual 2302	
Optimal design parameters	**value**
number of heat exchangers (n_{mod})	2
height of the top column (H_{top})	2.1 m
diameter of the top column (D_{top})	1.2 m
height of the bottom column (H_{bot})	1.7 m
diameter of the bottom column (D_{bot})	1 m
particle diameter (D_p)	0.26 mm
Objectives and constraints	**value**

S_{tot} (overall surface)	7.42 m^2
Temperature difference ($\lvert T_{3,sim} - T_3 \rvert$)	2.5 K
Predicted particle temperature at the outlet of the top column, $T_{p\_press,\ sim}$	1221 K

Table 8. Individual selected: geometric and thermal parameters

Fig. 12 refers to the top column of individual 2302; Fig. 12a shows the particles traces coloured by the particle temperature; Fig.12b shows the particles traces coloured by the particle velocity, whereas Fig. 12c shows the contours of gas temperature plotted along the symmetry planes.

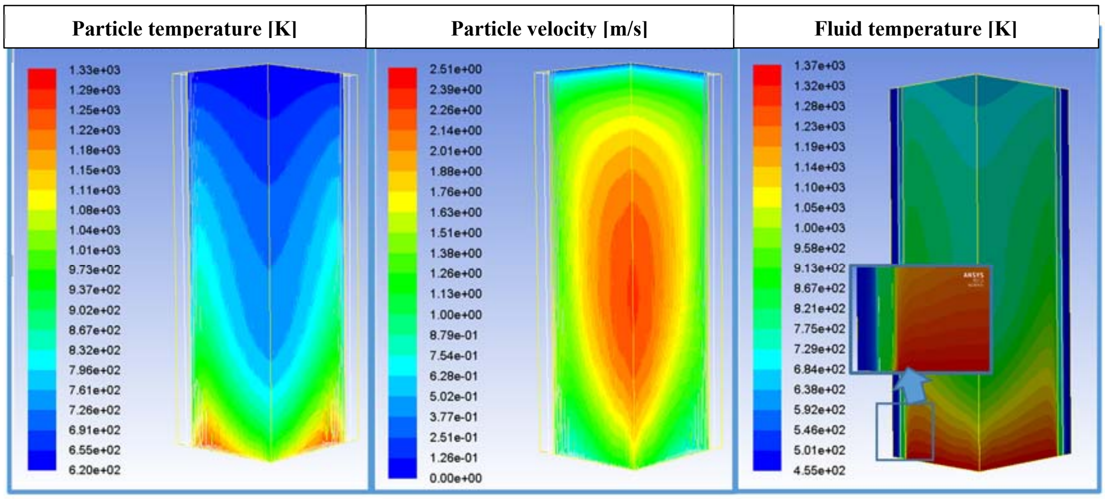

(a) (b) (c)

Fig. 12. Particle temperature (a), particle velocity (b) and gas temperature (c) of individual 2302 (top column)

Fig. 12a shows that the particles gradually increase their temperatures while descending to the bottom. The final average temperature of the particles is 1221 K (this temperature respects the prescribed constraint, see table 6). As shown in Fig 12b, the velocity of the particles increases while the particles are falling down because of gravity, with the maximum velocity being registered approximately at the centre of the column. After this, the particles slow down because the gas velocity increases from the bottom to the top of the column (because of the gas temperature profiles shown in Fig. 12c) until approaching the bottom of the column with an average velocity of about 0.5 m/s.

Similarly, Fig. 13 refers to the bottom column of individual 2302; Fig. 13a, 13b and 13c report, respectively, the particles traces coloured by the particle temperature, the particles traces coloured by the particle velocity and the contours of gas temperatures plotted along the symmetry planes. As shown in Fig. 13c, the compressed air enters the external channel surrounding the bottom column at the temperature of 502 K (which corresponds to the temperature at which it left the top column), flows through the internal channel and finally enters the bottom column through the internal channel. After having exchanged heat throughout its ascent, the compressed air reaches the average temperature of 1154.5 K at the exit of the top column. It is possible to observe both in Fig. 12c and in Fig. 13c that the internal wall temperature is maintained at low values, with the maximum temperature being predicted in the top column (as expected) with a value of about 870 K. This temperature is tolerable by most steels, also considering that the internal wall of the top column is subjected to a very low pressure gradient (3.5 bar). With regard to the pressure losses in both columns, they were predicted to be negligible, with the overall pressure drop suffered by the air from the inlet to the outlet of the IPHE being 49 Pascal only.

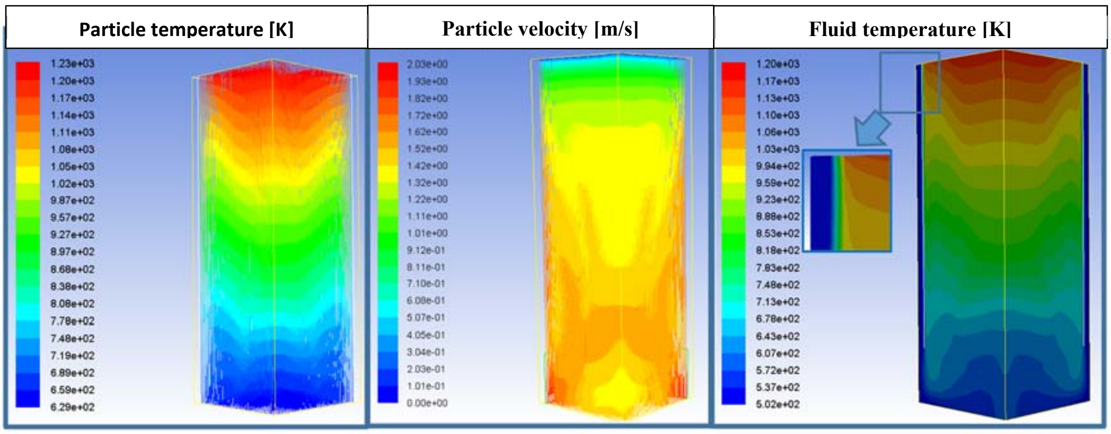

(a) (b) (c)

Fig. 12. Particle temperature (a), particle velocity (b) and air temperature (c) of individual 2302 (*bottom column)*

After having selected the number of heat exchangers, the geometrical values for both columns as well as the particle diameter, equations 1-3 can be used to design the three particle handling systems. The calculation of the volume of each rotor (*V*) can be achieved by using equation (1); however, the following parameters need to be fixed and/or determined before, specifically: rotational speed of the rotor (*n*) and filling coefficient (λ_v). With regard to the rotor speed (*n*), it must be kept quite slow, in order to ensure a good filling of the chambers; a value of 0.1 revolution/s was chosen for this calculation. With regard to filling coefficient (λ_v), it can be assumed equal to 0.5, as the particles are expected to occupy a half of each chamber in the case of a good filling. With these assumptions, the volume of each rotor results to be equal to *V*=0.002268 m^3. In addition, using a geometry having *h=W/2*, D_r*=W* and *ξ=0.8* (see equation 3) , it results that the width of the blades (*W*) is equal to 10.63 cm, the height (*h*) of the blades is 5.32 cm and the diameter of the rotor (D_r) is 10.63 cm.The main assumptions and geometric parameters are also reported in Table 9.

Rotary valve	value
n [rpm]	6
λ_v	0.5
ξ	0.9
Volume per revolution (V) [m^3]	0.002268
Blade width (W) [cm]	10.63
Blade height (H) [cm]	5.315
Rotor diameter (D_r) [cm]	10.63

Table 9. Rotary valve dimensions and parameters

With regard to the loss of compressed air, it can be calculated by using equations 4-6. Assuming that the pneumatic conveyor has an efficiency equal to η_{conv}=0.2 one obtains:

$$
\begin{aligned}
&G_{a,lost,1}=0.000481\ \text{kg/s} \rightarrow \frac{G_{a,lost,1}}{G_a}=0.0606\% \\
&G_{a,lost,2}=0.000614\ \text{kg/s} \rightarrow \frac{G_{a,lost,2}}{G_a}=0.0774\% \\
&G_{a,lost,3}=0.000614\ \text{kg/s} \rightarrow \frac{G_{a,lost,3}}{G_a}=0.0757\% \\
&G_{a,lost}=0.794\ \text{kg/s} \rightarrow \frac{G_{a,lost}}{G_a}=0.214\%
\end{aligned}
\tag{11}
$$

Table 10 reports the losses of compressed air for completeness. The sum of the three contributions shows that the overall loss of compressed air is absolutely negligible, being of the order of 0.2% of the overall compressed air delivered by the compressor.

Loss of compressed air	Value (%)
First contribution of loss of compressed air ($\frac{G_{a,lost,1}}{G_a}$) [%]	0.0606
Second contribution of loss of compressed air ($\frac{G_{a,lost,2}}{G_a}$) [%]	0.0774
Third contribution of loss of compressed air ($\frac{G_{a,lost,3}}{G_a}$) [%]	0.0757
Overall loss of compressed air ($\frac{G_{a,lost}}{G_a}$) [%]	0.214

Table 10. Losses of compressed air

Summarizing, the application of the approach described in section 2 has led to the conclusion that the IPHE should be split into two modules, with both being characterized by an overall height necessary for the heat exchange of 3.8 m (height of the top column plus height of the bottom column), with a maximum diameter of 1.2 m (representing the diameter of the bottom column). The particles should be manufactured with a diameter of 0.26 mm to make the above dimensions of the columns effective, thus achieving the desired heat exchange efficiency. As expected, because of the large difference in density between gas and ceramic particles, the three rotary valves result to be very small, with a volume per revolution of 0.002268 m^3. These data regard a specific case of application, namely a small scale combined cycle capable of generating an electrical power of 110 kWe and a thermal power of 234 kW, with an air mass flow rate of about 0.8 kg/s and a HTHE efficiency of 0.75. In these conditions, the size of the IPHE results to be quite compact, evidencing that its implementation into a real plant would not present particular issues in terms of dimensions. The low size is due to the high overall heat exchange coefficient that in turn results from the uniform dispersion of the thermal vector (the ceramic particles) within the gas stream. It should be noted that the increase in the heat exchange efficiency, η_{IPHE}, would require higher heights for the columns; however, the analysis reported in [11] demonstrated that the achievement of very high values for η_{IPHE} is not necessary, as the increase in η_{IPHE} causes a reduction in the gas temperature entering the HRSG. Furthermore, the CFD analysis of both columns has shown that the architecture proposed for both columns allows the temperature of the walls to remain within low values which are tolerable by most steels results. This feature is particularly important, because the use of steel for both columns (instead of ceramic material) can allow constructing the columns easily and with low costs. As a result, the manufacturing and assembly of the IPHE does not represent an issue, also considering that even the particle handling systems can be manufactured out of steel thanks to the architectures proposed. With regard to the loss of compressed air, it was demonstrated that only a negligible part (0.2% of the flow rate suctioned by the compressor) is lost because of the particle handling systems. In addition, the pressure drops caused by both columns is absolutely negligible. These results have shown that the project is highly viable, thus encouraging further studies and the forthcoming experimental validation of the project.

4. Conclusions

The aim of this paper was to propose a general approach for the design of the immersed particle heat exchanger (IPHE), suitable to external combustion plants using alternative or dirty fuels, such as carbon-neutral biomass. In particular, the focus was the application of the IPHE to a novel typology of small scale combined cycles proposed in previous studies. Taking advantages of the preliminary results achieved in previous studies, new technical solutions having general validity were studied, proposed and modelled in this paper. The immersed particle heat exchanger employs solid particles as an intermediate solid medium to transfer heat from the hot gases (exiting the external combustor at low pressure) to the compressed air (exiting the compressor at high pressure); because of this architecture, three particle handling systems plus a pneumatic conveyor are needed to move the solid medium between the two columns. The solution proposed for each particle handling system is mainly composed of a convergent reservoir, a guillotine valve and a rotary valve. With regard to the latter, it can be easily implemented into the IPHE because it is a component widely used in several industrial fields, allowing particles and loose material to be moved from two environments at different pressures, being mainly composed of a gear rotor spinning within a cover interposed between two environments at different pressure. Analytical models were developed that are based on simple equations allowing both the main dimensions of the particle handling systems to be determined and the loss of compressed air (due to the presence of these systems) to be estimated. Besides, a new architecture for both columns was conceived in this paper taking advantage of previous architectures presented in previous studies; the main difference is that the compressed air coming from the compressor, before entering the bottom column, is forced to flow through an internal channel comprised between the external casing and the walls of the columns. During this path, the compressed air cools the walls of the IPHE until reaching the inlet of the bottom column; this new solution has the potential not only to dramatically reduce the capital costs (by avoiding using ceramic and/or composite materials) but also to minimize the thermal dispersion towards the external environment. In respect of this new architecture, a thorough optimization design procedure was developed in this paper in order to select the optimum values of the IPHE modules, diameters and heights of both columns as well as the particle diameter that allow achieving the desired heat exchange efficiency. The optimization design is based on the interaction among simple analytical equations (allowing fixing some necessary thermal parameters), a genetic algorithm (MOGA II) and a thorough CFD analysis of the heat exchange between the particles and the gas within both columns. As far as the CFD modelling phase is concerned, only a quarter of the fluid domain was be meshed for both columns, taking advantage of the symmetry of the geometry. The main features of this CFD analysis (including geometry, zone types, boundary conditions, model and material properties) as well as the optimization strategy (including the characteristics of the optimization algorithm, constraints and objectives) were reported thoroughly.

The optimization procedure, which has general validity (in that it can be applied to different values of the parameters characterizing the combined cycle) was tested with application to specific values of thermal parameters and flow rates of a combined cycle capable of producing about 110 kW_e; in these conditions, the thermal efficiency of the IPHE is equal to 0.75. With regard to the result of the optimization procedure, it was found that the IPHE must be split into two modules having small size, showing the feasibility of the project in terms of dimensions. In addition, it was shown that the internal wall temperature is maintained within low values by virtue of the new architecture proposed, with the maximum temperature being predicted in the top column (as expected) with a value of about 870 K, allowing for the use of stainless steels instead of more expensive ceramic and/or composite materials. With regard to the loss of compressed air due to the employment of the particle handling systems, it was demonstrated, by using the proposed analytic equations, that overall loss of compressed air is absolutely negligible.

The application of the whole design procedure to a specific case has shown that project is highly viable; the next step will be the experimental validation of the entire project idea, with the construction of a pilot plant composed of an externally fired combined cycle coupled with the high temperature gas to gas heat exchanger (by means of a project funded by Apulia Region, at the LabZero Research Centre of Polytechnic University of Bari in the south of Italy).

In addition to demonstrating the viability of the project, this paper was aimed at providing the necessary tools and a general validity design procedure which can help other researchers and/or industrial manufacturers to design and construct prototypes of high temperature gas to gas heat exchangers to be applied to small scale externally fired gas turbines or combined cycles for the distributed energy generation from carbon-neutral biomass.

5. References

1. Vandyck, T., Keramidas, K., Saveyn, B., Kitous, A., & Vrontisi, Z. (2016). A global stocktake of the Paris pledges: Implications for energy systems and economy. Global Environmental Change, 41, 46-63.
2. Amelio, M., Ferraro, V., Marinelli, V., & Summaria, A. (2014). An evaluation of the performance of an integrated solar combined cycle plant provided with air-linear parabolic collectors. Energy, 69, 742-748.
3. Amirante, R., Cassone, E., Distaso, E., & Tamburrano, P. (2017). Overview on recent developments in energy storage: Mechanical, electrochemical and hydrogen technologies. Energy Conversion and Management, 132, 372-387.
4. Loha C., Chatterjee P.K., Chattopadhyay, H. (2011). Performance of fluidized bed steam gasification of biomass–modeling and experiment. Energy Convers Manage, 52(3):1583–8.
5. Loha, C., Chattopadhyay, H., & Chatterjee, P. K. (2014). Three dimensional kinetic modeling of fluidized bed biomass gasification. Chemical Engineering Science, 109, 53-64
6. Borsukiewicz-Gozdur A, Wis´niewski S, Mocarski S, Ban´ kowski M. ORC power plant for electricity production from forest and agriculture biomass. Energy Convers Manage 2014;87:1180–5.
7. Zhang C, Shu G, Tian H, Wei H, Liang X. Comparative study of alternative ORC based combined power systems to exploit high temperature waste heat. Energy Convers Manage 2015;89:541–54.
8. Dai Y, Wang J, Gao L. Parametric optimization and comparative study of organic Rankine cycle (ORC) for low grade waste heat recovery. Energy Convers Manage 2009;50(3):576–82.
9. Wei D, Lu X, Lu Z, Gu J. Performance analysis and optimization of organic Rankine cycle (ORC) for waste heat recovery. Energy Convers Manage 2007;48(4):1113–9.
10. Capata R, Toro C. Feasibility analysis of a small-scale ORC energy recovery system for vehicular application. Energy Convers Manage 2014;86:1078–90
11. Amirante, R., & Tamburrano, P. (2015). Novel, cost-effective configurations of combined power plants for small-scale cogeneration from biomass: Feasibility study and performance optimization. Energy Conversion and Management, 97, 111-120.
12. Amirante, R., Clodoveo, M. L., Distaso, E., Ruggiero, F., & Tamburrano, P. (2016). A tri-generation plant fuelled with olive tree pruning residues in Apulia: An energetic and economic analysis. Renewable Energy, 89, 411-421.

13. Rovense, F., Amelio, M., Ferraro, V., & Scornaienchi, N. M. (2016). Analysis of a Concentrating Solar Power Tower Operating with a Closed Joule Brayton Cycle and Thermal Storage. International Journal of Heat and Technology, 34(3), 485-490.
14. Soltani, S., Mahmoudi, S. M. S., Yari, M., & Rosen, M. A. (2013). Thermodynamic analyses of an externally fired gas turbine combined cycle integrated with a biomass gasification plant. Energy Conversion and Management, 70, 107-115.
15. Santos, M. J., Merchán, R. P., Medina, A., & Hernández, A. C. (2016). Seasonal thermodynamic prediction of the performance of a hybrid solar gas-turbine power plant. Energy Conversion and Management, 115, 89-102.
16. Jeong JH, Kim LS, Lee JK, Ha MY, Kim KS, Ahn YC. Review of heat exchanger studies for high-efficiency gas turbines. In ASME Turbo Expo 2007: Power for Land, Sea, and Air. American Society of Mechanical Engineers; January 2007. p.833–40
17. C. F. McDonald, Recuperator considerations for future higher efficiency microturbines, Applied Thermal Engineering, vol. 23, no. 12, pp. 1467–1487, 2003.
18. D. G. Wilson and J. M. Ballou, Design and performance of a high-temperature regenerator having very high effectiveness, lowleakage and negligible sealwear, in Proceedings of theASME Turbo Expo, pp. 183–197, Barcelona, Spain, May 2006.
19. B. J. Tsai and Y. L.Wang, "A novel Swiss-Roll recuperator for the microturbine engine," Applied Thermal Engineering, vol. 29, no. 2-3, pp. 216–223, 2009.
20. P. Zimmermann, A. Cardenas, C. Hirsch, and T. Sattelmayer, "Simulation of a micro turbine's dynamic behavior in a biomass incineration power plant based on the Pebble Heater technology," in Proceedings of the ASME Turbo Expo, vol. 5, pp. 93–102, Orlando, Fla, USA, June 2009.
21. D.Aquaro and M. Pieve, High temperature heat exchangers for power plants: Performance of advanced metallic recuperators, AppliedThermal Engineering, vol. 27, no. 2-3, pp. 389–400, 2007.
22. Amirante, R., & Tamburrano, P. (2014). High Temperature Gas-to-Gas Heat Exchanger Based on a Solid Intermediate Medium. Advances in Mechanical Engineering, 6, 353586.
23. Catalano, L. A., Amirante, R., Tamburrano, P., & Copertino, S. (2012). Analysis of the complementary energy losses of a high temperature gas to gas heat exchanger based on a solid intermediate medium. WIT Transactions on Engineering Sciences, 75, 109-120.
24. Catalano, L. A., De Bellis, F., Amirante, R., & Rignanese, M. (2011). An immersed particle heat exchanger for externally fired and heat recovery gas turbines. Journal of Engineering for Gas Turbines and Power, 133(3) doi:10.1115/1.4002157.
25. ANSYS FLUENT Theory Guide 14.0. November 2011. Fluent Inc.
26. Cengel YA. Introduction to thermodynamics and heat transfer. New York: McGraw Hill Higher Education Press; 2007. p. 253–62.
27. ModeFRONTIER™ User Manual. 2007. ESTECO s.r.l., AREA Science Park, Trieste, Italy. http://www.esteco.com Barbarelli,S., Amelio, M., Castiglione, T., Florio, G., Scornaienchi, N. M., Cutrupi, A., & Zupone, G. L. (2014). Analysis of the equilibrium conditions of a double rotor turbine prototype designed for the exploitation of the tidal currents. Energy Conversion and Management, 87, 1124-1133.
28. Amirante, R., Catalano, L. A., Poloni, C., & Tamburrano, P. (2014). Fluid-dynamic design optimization of hydraulic proportional directional valves. Engineering Optimization, 46(10), 1295-1314.
29. Amirante, R. & Tamburrano, P. (2016). Tangential inlet cyclone separators with low solid loading: Design by means of 3D fluid dynamic optimization. Engineering Computations, 33(7), 2090-2116.

Acknowledgments

The research presented in this work is funded by “Fondo di Sviluppo e Coesione 2007-2013 – APQ Ricerca Regione Puglia, Programma regionale a sostegno della specializzazione intelligente e della sostenibilità sociale ed ambientale - FutureInResearch”.